Target detection and recognition with polarimetric SAR

R.J. Dekker and A.C. van den Broek

TNO Physics and Electronics Laboratory, P.O. Box 96864, 2509 JG The Hague, The Netherlands

ABSTRACT

Target detection and recognition using polarimetric SAR data has been studied by using PHARUS and RAMSES data collected during the MIMEX campaign. Additionally very high-resolution ISAR data was used. A basic detection and recognition scheme has been developed, which includes polarimetric speckle-filtering, CFAR detection and the extraction of geometrical, intensity and polarimetric features. From the SAR images we conclude that polarimetric features can be useful to discriminate targets from clutter. At resolutions of 1 meter or better, shape and orientation recognition can be obtained with these features. To classify the targets, other features or other techniques have to be used. Examples are polarimetric decomposition techniques, of which two have been explored using the ISAR data.

Keywords: SAR, polarimetry, target detection, recognition, polarimetric decompositions

1. INTRODUCTION

The Royal Netherlands Army is currently introducing UAVs carrying electro-optical imaging sensors operating in the optical and thermal infrared wavelength region. Since also the need for an all-time and all-weather capability has been identified, interest for SAR imaging systems is growing. In this context a study was defined in which the role of SAR for ground surveillance has been investigated. In the study presented here we want to evaluate the role of high and medium resolution millimetre wave or microwave imaging systems for the purpose of military ground surveillance. We have therefore participated in the MIMEX campaign in order to survey military relocatable targets deployed at the UK Swynnerton test site. The campaign was prepared and conducted by the NATO research group AC/243 (Panel 3/RSG 20), predecessor of the present working group on MMW imaging techniques TG14.

With respect to military intelligence we distinguish between wide area surveillance with medium resolution SAR systems for the purpose of terrain interpretation and target detection, and target acquisition for the purpose of target detection, classification and recognition. We will focus here mainly on the target classification and recognition. The aspects of terrain interpretation and detection were discussed before.[1] For the study we have used data from the Dutch PHARUS polarimetric SAR and the French RAMSES high-resolution and polarimetric SAR, collected during the MIMEX campaign. We present the results of a target classification algorithm for the relocatable targets in the scene. The benefit of polarimetry at even higher resolutions has been investigated by using US fully polarimetric ISAR data.

The organisation of the paper is as follows. In section 2 we describe the data that was used. In section 3 we introduce a target detection and recognition scheme, which we applied to the SAR data. In section 4 we discuss polarimetric decomposition techniques, which we applied to the high-resolution ISAR data. Finally in section 5 we give conclusions.

2. DESCRIPTION OF THE DATA

During the MIMEX campaign (30 September to 25 October 1996) images were collected over the Swynnerton test site with various sensors. Five targets were deployed, including some relocatable rocket-launchers and a ZSU 23-4 tracked anti-aircraft vehicle. The Netherlands participated with the fully polarimetric PHARUS system, operating in the C-band. Images were successfully collected on 24 October 1996 for 3 tracks: two so-called long range (large incidence angles) images with perpendicular tracks, and one so-called short range image (small incidence angle). The long-range images have been used in this study because these images showed higher contrast due to longer shadows. Polarimetric calibration (i.e. phase calibration, cross-talk removal, and gain imbalance calibration) was done by using clutter statistics and antenna

Other author information: R.J.Dekker; Email: R.J.Dekker@fel.tno.nl; Telephone: +31 70 374 0431; Fax: +31 70 374 0654. A.C. van den Broek; Email: vandenBroek@fel.tno.nl; Telephone: +31 70 374 0430; Fax: +31 70 374 0654.

In *Radar Sensor Technology V*, Robert Trebits, James L. Kurtz, Editors, Proceedings of SPIE Vol. 4033 (2000) • 0277-786X/00/$15.00

measurements.[2] Absolute calibration was not performed. France participated with RAMSES (X, Ka and W band) which is operated by ONERA. It produces higher resolution images in all bands, see Table 1. Only the X-band system is polarimetric. The Ka and W band systems are single channel and have incidence angles comparable to that of the PHARUS system (75°). All images were processed with a maximum number of looks (Table 1). The numbers of looks of the polarimetric data is given by their polarimetric filtered images (see also section 3.1). Polarimetric calibration of the X-band data was done in the same way as the PHARUS data.

Polarimetric ISAR (i.e. inverse SAR) turntable data was provided by ARL. The data consists of six runs at three wavelengths and two incidence angles of a ZSU 23-4, which was one the relocatable target in the Swynnerton test area, see Table 2. The data has been processed using a two-dimensional FFT,[3] and cosine squared weighting (tapering 6 dB). We see that the incidence angle of 78° is comparable to the incidence angles of the C, Ka and W band data (Table 1).

Table 1. SAR data.

Party	TNO-FEL	ONERA		
System	PHARUS	RAMSES		
Band	C	X	Ka	W
Frequency	5.3 GHz	9.5 GHz	35 GHz	95 GHz
Polarisation	Quad (linear)	Quad (linear)	VV	LR
Altitude	3000 m	2400 m	900 m	900 m
Range	12000 m	3500 m	3500 m	3500 m
Incidence angle	75°	45°	75°	75°
Resolution	3.5 m	1.0 m	0.5 m	1.0 m
Number of looks	8 (PWF)	3 (PWF)	4	8

Table 2. ISAR data (δ_a stands for azimuth resolution).

Party	ARL		
System	Fully polarimetric stepped frequency radar		
Band	X	Ka	W
Centre frequency	9.25 GHz	34.25 GHz	94.25 GHz
Bandwidth	1511.64 MHz	1511.64 MHz	1511.64 MHz
Frequency step	5.928 MHz	5.928 MHz	5.928 MHz
Angle sampling interval	0.03°	0.015°	0.006°
Coherence interval (δ_a = 10 cm)	9°	2.4°	0.9°
Polarisation	Quad (linear)		
Depression angle	30° and 12°		
Incidence angle	60° and 78°		
Resolution	0.1 m		
Number of looks	Single Look		

3. DETECTION AND RECOGNITION SCHEME

An Automatic Target detection and Recognition (ATR) scheme is generally described by Fig. 2. Initially pre-processing is performed, which is often speckle filtering in case of SAR data. The second stage involves detection on the filtered image. Mostly a Constant False-Alarm Rate (CFAR) detector is used. Then the detected pixels are clustered into segments. After that several features are extracted for each segment, which are used to determine the nature of the segment. This can be to discriminate between targets and clutter, or between different types of targets. The latter obviously requires features extracted from higher resolution SAR data (less than 0.5 m). Note that Fig. 1 is a general scheme. Some authors came up with other schemes like Kreithen et. al.[4] They introduced a discriminator before the classifier, to reject natural-clutter false alarms. Sometimes it is recommended to reduce the number features with a Karhunen-Loeve transform.[5]

In this paper we have used a straightforward classification procedure to discriminate the relocatable targets from the natural-clutter false alarms. Due to the limited resolution of the SAR data, and the fact that we are dealing with a limited data-set,

we were not able to discriminate between the different types of the targets deployed during MIMEX campaign. Therefore we evaluated polarimetric decomposition techniques applied to the high-resolution ISAR data. Because ISAR data contains little clutter, pre-processing, detection and segmentation were omitted here. In the following we discuss each step in the detection and recognition scheme in more detail.

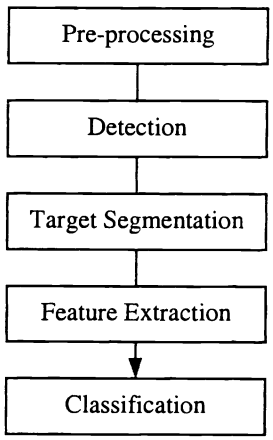

Figure 1. General ATR system.

3.1. Polarimetric filtering

Detection in SAR imagery is improved when speckle is reduced, since the signal-to-noise ratio increases for the target. We discriminate between polarimetric and spatial filtering. The first type of filtering has the advantage that the spatial resolution is not decreased. We therefore focus on the this type of filtering. Several filters were investigated.[1] The most optimal filter is the Polarimetric Whitening Filter (PWF). The essence of the filter is the transformation of linear polarimetric data with base (HH, HV, VV) to a base where the three polarimetric channels are not correlated. The filter produces a weighted average of these non-correlated channels. The filter for multi-look data is given by:[6]

$$y = tr\left(\Sigma_c^{-1}\Sigma\right) \tag{1}$$

Here Σ stands for the covariance matrix of the sample to be filtered, and Σ_c for the average covariance matrix surrounding the sample. $tr(\ )$ denotes the trace of a matrix. For Σ_c often a generic covariance matrix is chosen which is representative for most of the backgrounds of targets. The maximum increase of number of looks that can be obtained with a PWF filter is 3.

3.2. Detection

In the second stage the detection of pixels belonging to a potential target is performed. We have investigated a few CFAR detectors, in which the value of a sample of the target is compared with that of the average background clutter.[1] The hollow-stencil order-statistics CFAR detector[7] was preferred, because it gives better results producing less false alarms than the other CFAR detectors. It appears that the best results are obtained using the following CFAR equation:

$$\frac{x_t - x_{50}}{x_{80} - x_{20}} > K_{CFAR} \tag{2}$$

Here x_t stands for the sample to be tested and x_{50} for the median (50% value). x_{80} - x_{20} approximates the standard deviation (80% value minus 20% value). K_{CFAR} stands for the CFAR constant. The stencil is given by Fig. 2.

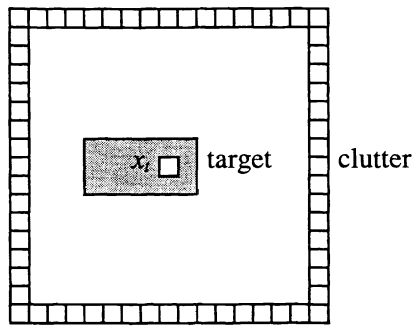

Figure 2. CFAR template with target.

To be able to compare the CFAR results of all images (PHARUS and RAMSES) we used the same CFAR detector, Eq. (2), with the same CFAR constant K_{CFAR} = 12.5. This value was chosen, since for this constant the false alarm rate due to speckle is negligible, and since the results on the basis of visual inspection of all images were optimal. The size of the template was in the order of 30 m for all images, see Table 4.

3.3. Target segmentation

In this stage the pixels that belong to one potential target are clustered. Segmentation is done by iterative merging of pixels or segments. The merge criterion, to decide if two pixels or segments belong to the same potential target, is given by the geometrical distance between the pair. The distance used in merging process was in the order of 1.5 m for all images.

3.4. Feature extraction

From all potential target segments a list of features was extracted, see Table 3. The list is subdivided in geometrical, radiometric and polarimetric features. We evaluated a feature by comparing it with a threshold, which was tuned to the actual targets in the images, since no independent training data to derive thresholds was available. The most powerful geometrical feature turned out to be the number of pixels n covering the target. Using this feature only, we were able to reduce the number of potential target segments with more than 90% (except for PHARUS), see Table 4. We introduced therefore a two-stage hierarchical classifier, evaluating the number of pixels n in the first stage, and evaluation of the other features in the second stage.

In the second stage the other geometrical features were analysed. The Minimum Bounding Rectangle (MBR, i.e. the rectangle which fits closest to the potential target) turned out to be not an effective feature. The ratio between n and the MBR (i.e. fill rate), and the length of a target segment were more appropriate for discrimination. The length was computed by averaging the distances between the top-left and bottom-right pixels, and between the top-right and bottom-left pixels, of a target segment. Its average direction was extracted as additional information, in case the (potential) target turns out to be a real one. Note that the direction becomes less accurate as the target becomes more horizontal or vertical oriented. Calculating the orientation by fitting a rectangular around the target, is possibly a better estimate of the direction.

Of the radiometric features, only the mean and the normalised variance (coefficient of variation) were appropriate for discrimination, except for PHARUS. Apparently the mean intensity for the real targets is significantly higher than that for false targets like trees. The minimum and maximum, their derived features, and the variance, appeared to be not appropriate for discrimination, as these features were quite variable for both the relocatable targets as the false alarms. The weighted-rank fill ratio[4] is a feature that is comparable to the variance. It is calculated by dividing the sum of intensities of the 5% brightest pixels, by the sum of intensities of all detected pixels. Despite the expectation of robustness it was not helpful here. Another feature, the fractal dimension[4] may perform better, but was not implemented for this study.

Polarimetric features could only be obtained from the fully polarimetric systems (RAMSES X-band and PHARUS C-band). These features were extracted from the average covariance matrix of the pixels covering a potential target. The powers and correlation coefficients in these matrices, appeared to be too variable to be discriminative. Also the angle of the co-polarised correlation coefficient, which is an indicator for the scatter-mechanism (even or odd bounce, see section 4), was too variable. Inspection of this angle for other man-made structures in the scene like buildings and fences, showed less variable

values for this angle. They were often close to 0° or 180°, in contrast to the values for the relocatable targets. The variability of this parameter for the targets is probably due to the complexity of the targets in combination with the resolution: if one resolution cell contains different kinds of scatter mechanisms, the observed angle is an average somewhere in the interval between 0° and 180°. Man-made structures like fences or buildings, probably show one dominant scattering mechanism (e.g. fence-ground or wall-ground, both double bounce). Also the power ratios HH-HV and HH-VV were not helpful for the same reason. When the scattering is due to several scatter mechanisms in one resolution cell the ratios become less pronounced and closer to 1. Only the power ratios in case of the X-band data turned out to be useful. The limited resolution of the PHARUS data was a problem using these features.

Table 3 shows interesting information, with respect to the polarisation used. Although the RAMSES W-band system has a lower resolution than its Ka-band system, it requires less features to discriminate the five relocatable targets form the clutter. This is possibly caused by its circular polarisation and the higher number of looks. Compared to the linear polarisation VV of the Ka-band system, the circular polarisation RL (i.e. right helix, left helix) of the W-band system is more sensitive to odd bounce scattering. This type of scattering is characteristic for flat plates and trihedral corner reflectors, see section 4. A fully polarimetric system, like the RAMSES X-band and the PHARUS system, has the advantage that every possible receive and transmit polarisation, linear or circular, can be obtained (section 4).

3.5. Classification

As described in the last section a two stage classifier was used. In the first stage the number of pixels n is evaluated and in the second stage the other features are evaluated. For operational real-time situations this can be interesting because it is computational quite efficient. Both stages contained simple and straight-forward processes in which the features are directly compared to a threshold. Some of the thresholds are given in Table 4. Because they were tuned separately for each image they are different. The tuned values for the thresholds of the area and length look realistic for the relocatable targets, except in case of the PHARUS data, which area threshold seem too high. No thresholds could be found that fit all images simultaneously. Secondly, we see that using the RAMSES images, all deployed targets could be found and all false alarms could be removed. Using PHARUS data some targets are missed and some false alarms stay detected. The only appropriate feature is the number of pixels used in the first stage. No other features used in its second stage are helpful. The reason for this is that its resolution of 3.5 m is probably insufficient, whether it is a polarimetric system or not. On the other hand, initially (after the first stage) the PHARUS images show the least number of false alarms. It must be noted that a sixth target (a radiometer platform) was deployed on the day PHARUS collected data. No system could make a distinction between targets. Therefore other techniques have to be studied. One is template matching, comparing the target segments with templates generated by measurements or signatures from target facet models.

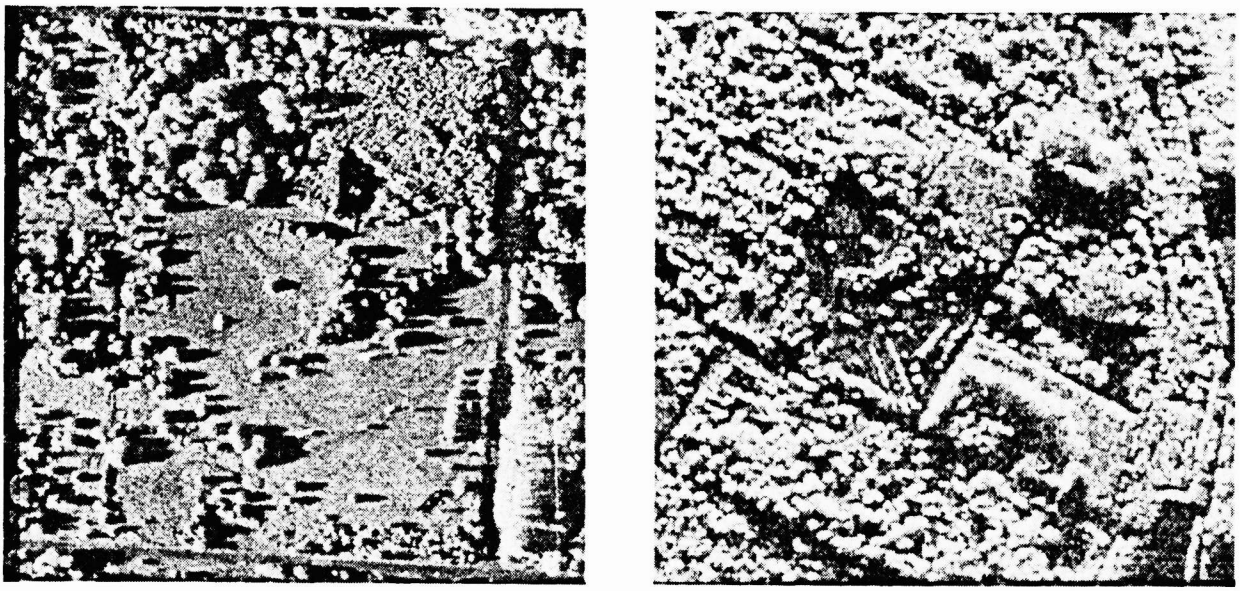

Figure 3. RAMSES Ka-band classified image (left): 5 targets out of 5; and PHARUS C-band classified image (right): 5 targets out of 6, 1 false.

Table 3. List of extracted features. A dot indicates that the feature was used to discriminate the target segments from clutter. A dot between brackets indicates that the feature could be used but was not necessary (W-band only).

Sensor	Ka	W	X	C	
Polarisation	VV	RL	4p.	4p.	
Resolution (m)	0.5	1.0	1.0	3.5	
Geometrical features					
n	•	•	•	•	Number of pixels covering the target
MBR					Number of pixels in minimum bounding rectangle
n/MBR	•	(•)	•		
Length	•	(•)	•		
Direction					Orientation target
Intensity features					On pixels covering target only
Maximum					
Minimum					
Mean	•	(•)			
Max/min					
Max/mean					
Variance					
Variance/mean^2	•	•			Normalised, known as coefficient of variation (cv)
Weighted-rank fill ratio					Ratio intensity brightest pixels/all pixels
Polarimetric features					On average covariance matrix of pixels covering target
Power HH ($S_{hh}S_{hh}^*$)	-	-			
Power HV ($S_{hv}S_{hv}^*$)	-	-			
Power VV ($S_{vv}S_{vv}^*$)	-	-			
Correlation HH-HV ($\|S_{hh}S_{hv}^*\|$)	-	-			Non-zero for rotated dihedral and dipole scattering
Correlation HV-VV ($\|S_{hv}S_{vv}^*\|$)	-	-			Non-zero for rotated dihedral and dipole scattering
Correlation HH-VV ($\|S_{hh}S_{vv}^*\|$)	-	-			
Angle HH-VV ($\angle S_{hh}S_{vv}^*$)	-	-			180° for dihedral (man-made) scattering
Ratio HH-HV ($S_{hh}S_{hh}^* / S_{hv}S_{hv}^*$)	-	-	•		Normalised
Ratio HH-VV ($S_{hh}S_{hh}^* / S_{vv}S_{vv}^*$)	-	-	•		Normalised

Table 4. Thresholds of some features, and the number of target segments left after classification stage 1 and 2. In the column of PHARUS (C-band) both long-range perpendicular images are given.

Sensor	Ka	W	X	C	
Resolution (m)	0.5	1.0	1.0	3.5	
Image size (m)	400	500	600	720	
CFAR size (m)	28	30	30	30	
Thresholds					
n max area (m^2)	26.4	32.5	47.3	90.0	
n min area (m^2)	7.2	12.5	12.3	45.0	
Length max (m)	9.0	9.3	14.7	-	
Length min (m)	5.8	4.8	5.1	-	
Numbers of targets					
Potential target detected	594	497	314	89/56	
Targets classified (stage 1)	44	36	14	6/6	After evaluating the number of pixels (*n*)
Targets classified (stage 2)	5	5	5	-	After evaluating the other features, see Table 3.
Real targets classified	5	5	5	3/5	RAMSES out of 5, PHARUS out of 6
False targets classified	0	0	0	3/1	

4. POLARIMETRIC DECOMPOSITIONS

In the previous section we studied straight forward polarimetric features, directly taken form the covariance matrix. In order to derive features more directly related to the scatter mechanisms, polarimetric decomposition techniques can be used. Polarimetric decompositions can be divided in stochastic or coherent.[4, 8-12] Stochastic decompositions are useful when the average (multi-looked) covariance matrix of a target is observed, but when single-look high-resolution data is available it is more interesting to use a coherent decomposition. The latter can be applied directly to the scattering matrix (i.e. Sinclair matrix). A decomposition resolving for the basic scatter mechanisms even and odd bounce, is given.[4] Even and odd stand for the number of times the signal reflects against a surface before it is send back. An example of an even bounce scatterer is a dihedral reflector. Examples of odd bounce scatterers are a sphere, a flat plate and a trihedral reflector. The decomposition is best described in the circular basis, which is given by:[12]

$$\begin{aligned} S_{RR} &= \frac{(S_{HH} - S_{VV})}{2} + i S_{HV} \\ S_{RR} &= \frac{(S_{HH} - S_{VV})}{2} - i S_{HV} \\ S_{RL} &= \frac{(S_{HH} + S_{VV})}{2} \end{aligned} \tag{3}$$

The even/odd decomposition is then given by:[4]

$$\begin{aligned} even &= \frac{|S_{RR}| + |S_{LL}|}{2} \\ odd &= |S_{RL}| \end{aligned} \tag{4}$$

From the linear point-of-view we see that in case of even bounce scattering HH and VV are 180° out of phase. In case of odd bounce they are in phase. Another coherent decomposition is given by Krogager,[11-12] who decomposes the even bounce component further in diplane (i.e. dihedral) and helix (i.e. circular dipole):

$$\begin{aligned} k_d &= |S_{LL}|, k_h = |S_{RR}| - |S_{LL}| \quad \text{if} \quad |S_{RR}| > |S_{LL}| \\ k_d &= |S_{RR}|, k_h = |S_{LL}| - |S_{RR}| \quad \text{if} \quad |S_{LL}| > |S_{RR}| \\ k_s &= |S_{RL}| \end{aligned} \tag{5}$$

Here k_d stands for diplane, k_h for helix and k_s for sphere (i.e. flat plate). Note that k_s is equal to the odd component in Eq. (4). Helix scattering is not only generated by a circular dipole. Two or more diplane scatterers in one resolution-cell may also result in helix scattering.[12] Therefore diplane scattering can be regarded as pure double-bounce and helix scattering as a more complex type of scattering. To compare both decompositions, high-resolution ISAR data of ARL was used. Figure 5 shows a W-band ISAR image (12° depression angle) of the ZSU 23-4, including a photo taken from nearly the same angle.

From the ISAR image series, the following features were used: *total energy*, *percent pure* (even, odd, diplane, etc.) and *percent bright*.[4] The *percent pure* feature stands for the fraction of all pixels within the target area, for which the main fraction of energy is even, odd, diplane, helix or sphere. The *percent bright* feature stands for the fraction of brightest pixels (i.e. CFAR image) within the target area for which the main fraction of energy is even, odd, diplane, etc. The features were obtained for the whole range of aspect angles. Some *pure* and *bright* ISAR images were selected to view where the scatterers are located. Figure 5 and 6 show the *percent bright* even and odd, respectively diplane, sphere and helix of the W-band ISAR series for the 12° depression angle. From both figures we see that the components fluctuate significantly, and that the helix component is small. We also see that the diplane component is often smaller than the even component, compared to odd or sphere, due to the helix scattering. Only at some angles diplane and helix are comparable. It is therefore questionable if the decomposition proposed by Krogager has an advantage in case of *percent pure* or *bright* measurements. Perhaps it is better not to decompose the even bounce component further. Additional research, e.g. studying other features,

will be necessary to confirm or refute this. On the other hand, if we view some *pure* and *bright* ISAR images, we see that helix scattering is often generated by more complicated structures. Some images for instance, show helix scattering from the tracks and from the cavity where the guns come out of the turret. This supports the idea that helix is a more complex type of scattering. The Krogager decomposition can be used in combination with classification by template matching, which possibly gives better results. However, for this purpose it is necessary to study more measurements from more different targets. Since the effort to obtain such data can be elaborate, ISAR signatures obtained from data generated using a RCS prediction code in combination with target facet models, can be a solution.

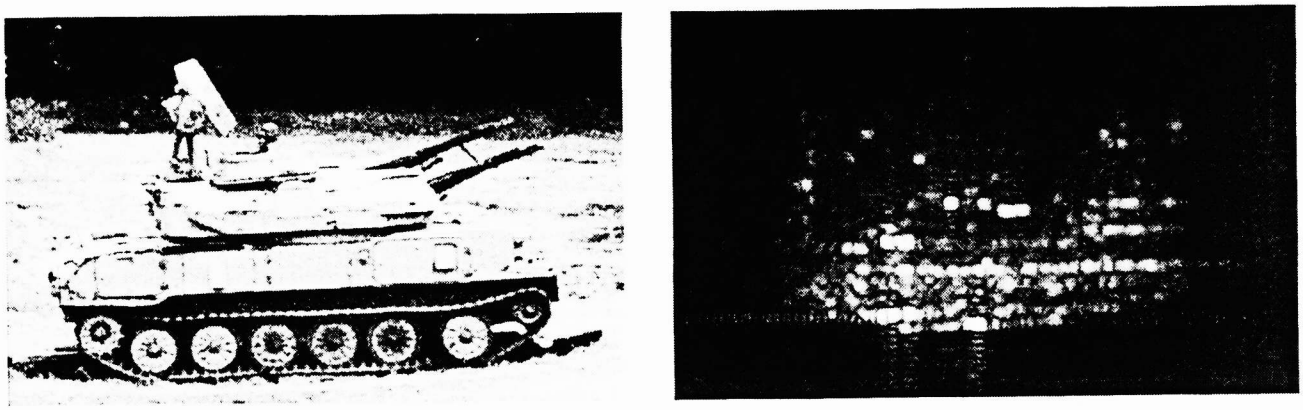

Figure 4. ZSU 23-4 tracked anti-aircraft vehicle on the ARL turntable and corresponding ISAR image (W-band, 12° depression angle).

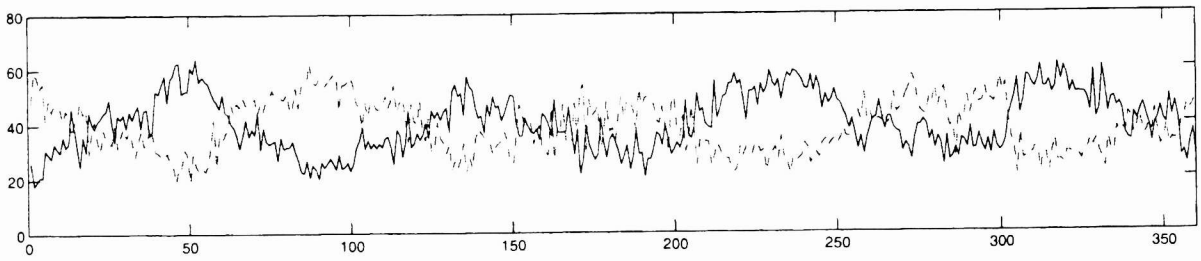

Figure 5. Percent bright even (solid) and odd (dashed), as a function of the orientation angle (W-band, 12° depression angle).

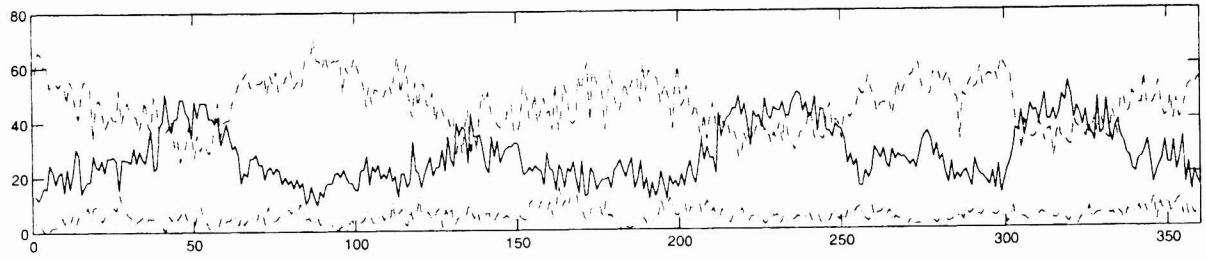

Figure 6. Percent bright diplane (solid), helix (dot-dashed) and sphere (dashed), as a function of the orientation angle (W-band, 12° depression angle).

5. CONCLUSIONS

In this paper we have presented results of our work concerning automatic target detection and recognition with polarimetric SAR data. A basic detection and recognition scheme was developed, including polarimetric speckle-filtering, CFAR detection and the extraction of geometrical, intensity and polarimetric features. The SAR data that were used varied from single polarisation linear and circular to fully polarimetric data with a resolution of 0.5 to 3.5 m. For the study of

polarimetric features in particular, we also used high resolution (0.1 m) ISAR data in combination with polarimetric decompositions.

From the SAR images of a scene containing five relocatable targets, we conclude that next to geometrical and intensity features, polarimetric features based on the covariance matrix, can be useful to discriminate the targets from clutter. The resolution must be about 1 m or better. In that case, size and orientation recognition of the target is possible. To discriminate between targets, other features and other techniques should be used. One potential technique comprises polarimetric features derived from polarimetric decompositions. Polarimetric decompositions in combination with template matching can be more efficient. In order to study the robustness of features with respect to the orientation of targets, and to study the potential to discriminate between targets, more and different-target data-sets are needed. These data-sets should preferably be polarimetric. One way of obtaining such polarimetric data-sets is to use a RCS prediction code in combination with facet models.

REFERENCES

1. A.C. van den Broek, R.J. Dekker, A.J.E. Smith, and F.P.P. de Vries, "Target detection with polarimetric C-band SAR", *Proc. Of the RTO Sensors and Electronics Technology Panel (SET) Symp., High Resolution Radar Techniques, Granada, Spain, 22-24 march 1999*, RTO-MP-40, AC/323(SET)TP/8, p. 56, 1999.
2. R.J. Dekker and A.C. van den Broek, "Calibration of Polarimetric PHARUS Data", *Proc. Of the CEOS SAR Workshop, Noordwijk, The Netherlands, 3-6 February 1998.*
3. C.C. Chen and H.C. Andrews, "Multifrequency Imaging of Radar Turntable Data", *IEEE Trans. on Aerosp. Electron. Syst., Vol. 16, No. 1*, pp. 15-22, 1980.
4. D.E. Kreithen, S.D. Halversen, and G.J. Owirka, "Discriminating Targets from Clutter", *Lincoln Laboratory Journal, Vol. 6, No. 1*, pp. 25-52, 1993.
5. R.O. Duda and P.E. Hart, *Pattern Classification and Scene Analysis*, John Wiley and Sons, New York, 1973.
6. G. Liu, S. Huang, A. Torre, and F. Rubertone, "The Multilook Polarimetric Whitening Filter (MPWF) for Intensity Speckle Reduction in Polarimetric SAR Images", *IEEE Trans. On Geosci. Remote Sensing, Vol. 36, No. 3*, pp. 1016-1020, 1998.
7. L.M. Novak and S.R. Hesse, "On the performance of order-statistics CFAR detectors", *IEEE Conference Record of the 25th Asilomar Conference on Signals, Systems and Computers, Vol.2*, pp. 835-840, 1991.
8. S.R. Cloude and E. Pottier, "A Review of Target Decomposition Theorems in Radar Polarimetry", *IEEE Trans. On Geosci. Remote Sensing, Vol. 34, No. 2*, pp. 498-518, 1996.
9. Y. Dong, B.C. Forster, and C. Ticehurst, "A New Decomposition of Radar Polarization Signatures", *IEEE Trans. On Geosci. Remote Sensing, Vol. 36, No. 3*, pp. 933-939, 1998.
10. A. Freeman and S.L. Durden, "A Three-Component Scattering Model for Polarimetric SAR Data", *IEEE Trans. On Geosci. Remote Sensing, Vol. 36, No. 3*, pp. 963-973, 1998.
11. E. Krogager, *Aspects of Polarimetric Radar Imaging*, Doctoral Thesis, Technical University of Denmark, Copenhagen, 1993.
12. E. Krogager and W.M. Boerner, "On the Importance of Polarimetric Information in Radar Imaging and Classification", *Proc. Of the AGARD Sensor and Propagation Panel Symp., Remote Sensing: A Valuable Source of Information, Toulouse, France, 22-25 April 1996*, AGARD-CP-582, p. 17, 1996.